Tsetse Wing Morphology Dynamics: Automated Landmark Detection and Time Series Analysis

Moegamat Nuhr Ryklief

Supervisors: Dr P Landi, Prof. W Brink, Prof. J Hargrove

Abstract: This study uses machine learning techniques to automate the identification of landmarks on the wings of tsetse flies by analysing a large dataset of wing images from Zimbabwe. The study obtains a high degree of accuracy in identifying wing landmarks by using a two-tier approach that includes convolutional neural networks ResNet50 for landmark detection and VGG16 for wing classification with a R^2 score of 0.8459. The paper explores the correlation between environmental factors and wing morphology through the application of time series analysis for automatic identification. Adaptive responses to environmental changes are revealed by the significant correlations between wing length and factors such as temperature and humidity. This novel method not only enhances the precision of morphometric analysis in vector biology but also provides insight into the ecology and evolution of tsetse flies, which could potentially influence disease control strategies in the context of climate change.

1. Introduction

The application of morphometric analysis in medical entomology has proven to be an essential tool **[1]** for understanding the dynamics of disease vectors and their adaptations to changing environments. Morphometrics is valuable in the study of tsetse flies, since it helps analyse and differentiate between the species and populations. *Trypanosomiasis*, a disease that substantially compromises human health and stunts agricultural growth in sub-Saharan Africa, has been transmitted by the tsetse (Figure 1) since 1896 **[2]**. Annually, African nations incur billions of dollars in treatment and preventive expenses **[3]**. An accurate understanding of the ecology and behaviour of tsetse flies is essential for the development of effective population control strategies that reduce the spread of disease.

Figure 1: The tsetse fly (*Glossina spp*) **[23]**

1.1. Tsetse

The three tsetse fly species, *Glossina morsitans*, *G. palpalis* and *G. fuscipes* are the primary vectors of African trypanosomiasis. They transmit the *Trypanosoma* parasites which cause sleeping sickness in humans and Nagana in animals **[4]**. The flies inhabit the tropical and subtropical regions of Africa, where they thrive in the humid conditions of savannas and riverine habitats **[5]**.

The tsetse flies exhibit distinctive morphological features, particularly in their wings, which are crucial for species identification. The wings are identified by their unique venation pattern and dimensions, which are subject to significant variation among varied species. For example, the wings of *G. morsitans* are longer than those of *G. palpalis*, which is a physical characteristic that is frequently employed in taxonomic research **[6]**. The sustenance of the tsetse flies is composed of the blood of their vertebrate hosts, which include humans, cattle, and other wild animals. These blood supplies are essential for larval manufacture during their reproductive cycle **[7]**.

Tsetse flies discharge the *Trypanosoma* parasites into the bloodstream of their hosts during their feeding process when they are bitten. The flies re-acquire the parasites from ill individuals or animals. Their behavioural patterns, which encompass strategies for locating hosts and migratory patterns, significantly influence transmission dynamics. Studies suggest that their migratory habits are closely associated with seasonal fluctuations and that their choice of hosts is determined by olfactory and visual signals **[8]**. In periods of drought, they may migrate toward water sources; however, during rainy seasons, they expand their range **[5]**.

1.2. Trypanosomiasis

The vector-borne trypanosomiasis disease, commonly referred to as sleeping sickness in humans and Nagana in animals, is caused by protozoic Trypanosoma parasites. Human African trypanosomiasis

(HAT) is caused by *Trypanosoma brucei gambiense* and *T. b. rhodesiense*, whereas animal trypanosomiasis is caused by *T. b. brucei* **[2]**. The disease symptoms form two stages. The first stage's symptoms include fever, headaches, enlarged lymph nodes, joint pains and itching. The second stage's symptoms are neurological: confusion, sensory disturbances, poor coordination and, most prominently, sleep cycle disturbances **[2]**. The effects on livestock are decreased productivity and increased mortality rates.

Diagnosis of trypanosomiasis requires screening with serological tests and microscopic examination of blood or lymphatic fluid to identify the parasites **[2]**. For effective treatment, early detection is essential, given the disease's rapid progression, which can become fatal if not treated.

Trypanosomiasis is exclusively a disease that affects regions where tsetse insects are prevalent, which encompasses 37 African countries. Healthcare expenses and cattle fatalities have a substantial economic impact on the African economy, with an estimated annual cost of USD 4.75 billion, according to the Food and Agriculture Organization (FAO) for 2024 **[3]**. The illnesses affect 50 million cattle and 60 million humans annually, resulting in approximately 3 million livestock deaths. The most severe consequences are experienced by rural communities where cattle are the primary source of income.

1.3. Tsetse fly research

The study of tsetse flies has made significant progress in the past few decades, largely due to the extensive collection efforts conducted in Zimbabwe. One notable endeavour at the Rekomitjie Research Station in the Zambezi Valley is the systematic collection of tsetse flies over a period of more than 11 years **[9]**. This initiative endeavoured to establish an exhaustive dataset. To optimize capture efficiency, this investigation has implemented numerous trapping strategies, including vehicle-mounted electric targets and odour-baited traps **[9]**. The collection technique's meticulous design is essential for future research, as it ensures the procurement of a representative sample of the tsetse population **[9, 10]**.

In addition to their wings, the 28 ordered volumes of tsetse flies contained numerous pages of exhaustive biological data. To ensure the preservation of the morphological integrity of tsetse fly wings, meticulous handling and storage methods were implemented. The distance between markers **a** and **b** (Figure 2) is a particularly intriguing measurement. This measurement is preferred over the hatchet cell length between markers **b** and **c** used in previous studies **[11]** because its longer distance reduces the relative error arising from variation of vein thickness **[9]**. This meticulous structuring of volumes ensures accurate data collection and organized access to the data **[10]**.

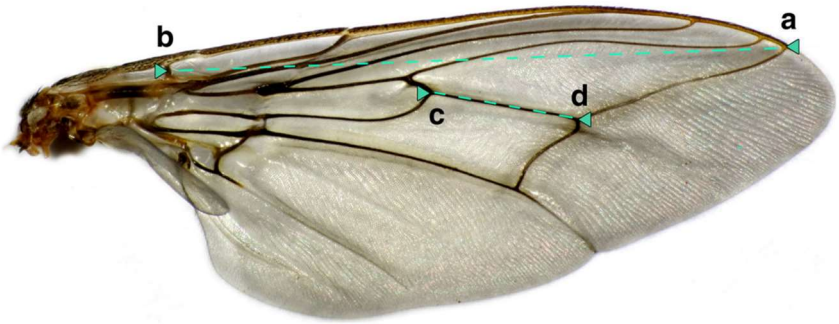

Figure 2: A right-wing image of a female *G. m. morsitans* with labelled endpoints **a** and **b**, showing wing length used in present studies, and points **c** and **d**, depicting hatchet cell length used in previous studies **[9]**

1.4. Analytical morphometry

Morphometric analyses are particularly effective quantitative instruments for examining morphological changes in organisms in relation to their environment, particularly for disease vectors. It is beneficial to evaluate and contrast morphological characteristics, thereby providing a comprehensive analysis of the ecological reactions and evolutionary adaptations of species **[1]**. Morphometric methods were employed in previous research to identify species and assess population structures to implement effective disease control measures **[12]**. Geometric morphometrics enable scientists to document the complex morphological changes in biological forms using sophisticated statistical methods **[13]**.

The measurement of linear Cartesian distances between wing landmarks is a significant application of morphometrics in the study of tsetse wing lengths. These measures can be compared to assess their influence on morphological characteristics by utilising environmental variables such as temperature and humidity **[10]**. These investigations would provide valuable insights into the adaptive strategies that tsetse flies employ in response to environmental changes.

1.5. Deep learning for landmark detection

Machine learning (ML) is a subset of artificial intelligence that is concerned with the development of statistical models and algorithms that enable computers to perform specific tasks without explicit instructions. Rather, these systems acquire knowledge from data, identifying patterns and making precise predictions based on the input they receive **[14]**. The application of machine learning can facilitate the rapid and straightforward identification of morphological data, including wing form and size, across vast datasets. This is particularly useful in the study of tsetse flies, where manual annotation would require a significant amount of time and effort. The capacity of ML to accurately categorize and forecast the traits of tsetse flies based on their wing form is a critical factor in the comprehension of larger-scale tsetse population dynamics **[10]**.

In a previous study **[10]**, an autonomous morphometric measuring method was developed using convolutional neural networks (CNNs) to investigate tsetse wing subsets. The system was capable of accurately determining the Cartesian coordinates of eleven wing landmarks that were consistent across all wing specimens. These loci are essential identification points that offer a comprehensive understanding of the size and form of tsetse wings. They have been employed in numerous morphometric studies of tsetse wings **[1, 5, 6, 9, 10]**. Figure 3 illustrates a wing image with its 11 landmarks superimposed on it. As before, the distance between points 1 and 6 is of particular importance.

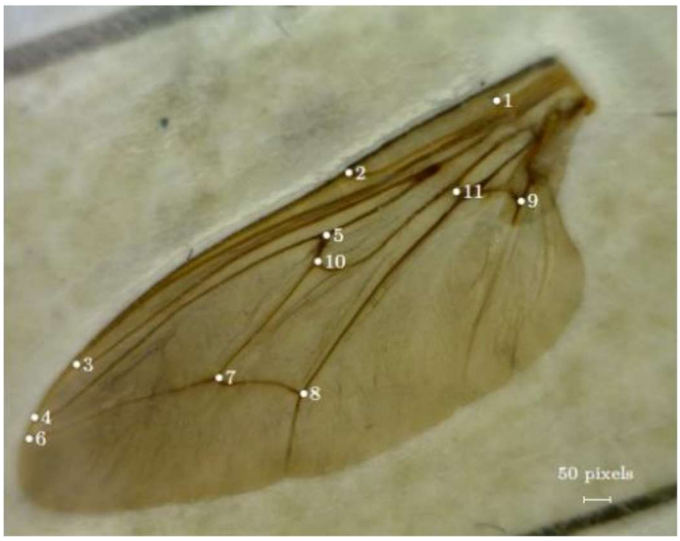

Figure 3: Image of a tsetse wing showing 11 landmarks identified by white numbered points. **[10]**

1.6. Convolutional neural networks

Convolutional neural networks have emerged as a cornerstone of modern computer vision, significantly enhancing the accuracy of landmark localization, object detection, and picture categorization. CNNs employ the spatial structure that is inherent in data types to explicitly handle data with a grid-like architecture, such as photos. The convolutional layer is the fundamental building block of a CNN, as it applies a collection of learnable filters (or kernels) to the input image, thereby emphasizing various aspects of the input data **[15]**.

To determine the most effective architecture for landmark detection in tsetse wing images, numerous CNN models were examined in a study **[10]** within the context of tsetse fly research. The study employed a two-tier approach, initially employing a classification model to identify entire wings and subsequently employing a regression model to identify landmarks on those wings. This method was ideal for addressing the challenges posed by fragmentary specimens; without correction, these would result in errors in landmark identification.

This systematic two-tier approach yielded a comprehensive dataset of landmark detections with accurately annotated tsetse wing images, which may provide valuable insights into the morphological diversity of tsetse populations. The integration of machine learning with morphometric analyses will enhance the robustness of species identification and facilitate the development of targeted control strategies for trypanosomiasis.

1.7. Research objectives

The objective of this study is to assess the repeatability of the deep learning approach of Geldenhuys et al. **[10]** for the automatic detection of landmarks in additional subsets of tsetse wing photographs. In particular, the data subset of Volume 22 will be employed to implement their two-tier technique, which employs CNNs. The initial classification of entire wing images will be based on the pre-trained VGG16 model in this regard. The regression challenge of 11 wing landmark location prediction will be conducted using the ResNet50 model following this phase.

Thorough morphometric studies over multiple volumes of wing images will be facilitated by the effective implementation of these techniques in increasing the landmark collection. We will assess the correlation between the manually measured wing lengths and the machine predicted wing lengths for Volumes 20 to 22 by utilizing the enlarged wing landmark data. This analysis will identify and exclude errors that stem from both manual measurements and deep learning predictions, thereby minimizing any discrepancies that could potentially undermine the validity of the morphometric data.

The extended landmark data will be employed in a time-series analysis to evaluate the dynamic changes in tsetse wing morphology over time in relation to shifting environmental variables. This comparative study has the potential to offer new insights into the evolutionary biology of tsetse flies and the potential responses of their morphological adaptations to environmental demands. These findings should be able to inform the development of policies for the control of tsetse populations, thereby facilitating the management of vector-borne illnesses.

1.8. Hardware and software

The coding was performed on an Intel(R) Core(TM) with a 3GHz i5-9500 CPU and 8GB RAM. All code was written in the Python 3.11.7 language using Jupyter Notebook. The pre-trained CNN models from the Pytorch Computer Vision Library were used and adjustments in their architecture were made to

suit the study requirements. The data related to the previous application of the two-tier approach can be found on Dryad **[16]** and the code in the GitHub repository **[17]**. Similarly, the data and code for the current study can be found in their own repositories **[18, 19]**.

2. Two-tier deep learning approach

The two-tier deep learning approach represents a methodology aimed at enhancing the accuracy of automated landmark detection in tsetse wing images. This approach is inspired by the CNN frameworks established by Geldenhuys, whose implementation on the Volumes 20 and 21 provide essential templates for implementation **[20]**. The effectiveness of CNNs in biological contexts have been proven in its use in previous applications for classification of insect images, strengthening their relevance in morphometric studies.

The two-tier system forms two parts. The first tier uses the VGG16 model to identify and remove incomplete wing images from complete ones. The second tier uses the ResNet50 model to predict the image coordinates of landmarks on the wings classified as complete **[10]**. Considering only the complete specimens for analyses results in the improved reliability of landmark detection. If incomplete specimens are removed correctly, the predicted landmark dataset is expected to produce accurately annotated wing images. These findings would provide useful insights into the morphological diversity of tsetse populations on a large **[10]**.

The performance of the CNNs are, however, highly dependent on the good quality training data. Poorly structured training sets would bias the model predictions and reduce its accuracy **[10]**. The models would also require considerable computational power and processing time, since they would need to learn more information from bad data. The augmentation of training data before model implementation would help in resolving these issues.

2.1. Data description

The collection of 362,186 tsetse fly specimens captured at the Rekomitjie Research Station A foundation for this tsetse research has come from. The wings of each fly were methodically secured to the lines of the pages in each volume using transparent adhesive tape. Biological measurements, including wing lengths were recorded for the right wing of each fly, measured manually in centimetres with a stage micrometer, maintaining data consistency and precision **[9]**.

The data subset employed for wing classification and landmark prediction is derived from Volume 22 of the collected specimens, spanning from August 1996 to February 1997. This subset was selected for its reasonably complete structure and scale, where there weren't extensive data quality issues needing to be addressed, making it suitable for investigating temporal changes in wing morphology. This volume makes up 377 pages, each accommodating a maximum of 20 lines. A total number of 7,443 flies with a maximum of 14,886 wings form the data content. Each line in a page represents one fly, with its corresponding biological data and wing sets taped to the line. The right-wing lengths were measured in centimetres using a binocular microscope, ensuring high accuracy in the measurements **[9]**. The pages were further laminated to preserve their structural integrity for future analyses.

Using a high-resolution microscope camera, the digitalisation procedure involved the acquisition of biological data and high-quality images of the wings at a resolution of 1,024 x 1,280 pixels. The images were meticulously organized into categories that corresponded with the structure of Volume 22. Images were named according to the fly wing's physical location within the volume. An example of an image label is V22P779L, which indicates that the corresponding fly is in Volume 22, Page 779, Line 4

and it is a left wing. This method of systematic naming enables rapid access and connection of images to their corresponding biological information.

For the training of the classifier model, data subsets of pre-classified wing images from the previous study **[10]** were selected. The two subsets consisted of an even class distribution of 600 wing images, where the first class of complete wing images contains all 11 landmarks, and the second class of incomplete wing images has missing landmarks 4 or 6. Compiling these data samples was simplified by using preexisting information on the number of missing landmarks in wings from the biological data set by visual inspection. A data-centric approach was used, focusing on consistent labelling, so that the training set wing categorised into well-defined groups. Images are labelled 1 for incomplete wings and 0 for complete wings **[10]**. The accompanying spreadsheet for Volume 22 contains 7,443 row instances, each corresponding to a fly. The variables included in the dataset are listed in Table 1.

Table 1: Biological data captured in lab dissection

Variable name	Description
vpn	Volume, page and number (e.g. 22077904)
g	Genus of the fly: 'Gp' for *G. pallidipes* or 'Gmm' for *G. m. morsitans*
s	Sex: 1 for male, 2 for female
hc	1 if hatchet cell used, 0 if distance landmarks 1 to 6 used
wlmm	Manually measured right wing length from landmarks 1 to 6 in cm, otherwise hatchet length
f	Wing fray category, approximating age (1 – 6)

Despite the dataset being thorough, it holds several errors that would impact the morphometric analysis quality, such as wing damage, missing wings, misalignment during imaging, and variations in image size and quality. Incomplete wings, which may lack important anatomical characteristics, would cause erroneous landmark identification in consequent analyses **[10]**. The dataset is further complicated by the absence of wings, which results in voids in the morphological data.

Misalignment may result in errors during the imaging process, as wings may not be captured in a consistent orientation, thereby affecting the precision of landmark placement. Additionally, variations in image size and quality, such as those associated with focus, luminance, and contrast, impede the functionality of automated detection systems. These issues necessitate a meticulous examination of the dataset to identify and eliminate partial wings, thereby ensuring that only complete specimens are considered when constructing morphometric data.

These obstacles should be addressed through data pre-processing and augmentation to enhance the model's visibility of the wing features for improved precision.

3. Tier 1: Incomplete wing classifier

3.1. VGG16 Model

The deep architecture VGG16 model balances complexity and efficiency within the perspective of image classification. It extracts complex characteristics from images with the assistance of the convolutional and completely connected layers. The model can learn high-level concepts without a significant increase in computational costs by progressively deepening the network with tiny convolutional filters of size 3 x 3 **[15]**.

The VGG16 architecture is initially constructed with a max pooling layer, followed by convolutional layers that employ 3 x 3 filters, starting with compressed input images of 224 x 224 pixels. The convolutional filters at each successive level are enhanced by the multiple pattern repetitions, resulting in three completely connected layers. The Rectified Linear Unit (ReLU) function introduces non-linearity in the model by operating on each convolutional layer. The architecture can be summarized as follows:

1. **Convolutional Layers**: Small 3 x 3 filters used for convolution are expressed as:

$$S(i,j) = (I * K)(i,j) = \sum_m \sum_n I(m,n)K(i-m, j-n)$$

where S is the output feature map, I is the input image, and K is the convolution kernel. By aggregating (max pooling), spatial dimensions can be reduced, allowing for the condensing of characteristics without sacrificing critical information.

2. **Max Pooling**: facilitated by convolutional layers, which aggregate feature maps. The process can be defined as:

$$P(i,j) \; = \; max\_\{m,n\}\, S(i+m, j+n)$$

This pooling method significantly enhances the abstraction capacity of the model by grouping the most critical elements and thereby reducing computational complexity

3. **Fully Connected Layers**: After the pooling layers, the model shifts to fully connected layers that work on a flattened version of the pooled feature maps. The softmax activation function is used to create probability distributions across multiple classes, developing into the final fully connected layer output that is suitable for classification problems.

To reduce a loss function, the VGG16 model is trained using optimisation techniques and categorical cross-entropy for multi-class classification. The backpropagation method is used to calculate the gradients of this loss function, allowing the network to adjust its weights.

The learning and design features of the VGG16 model are particularly appreciated in this work, as they assist in the classification of tsetse wing images into full and fragmented groups through hierarchical feature representations. The model's depth enables the identification of minute morphological variations that define entire specimens, such as the presence of specific landmarks **[15]**.

The VGG16 model is a critical element of the two-tiered strategy for tsetse wing research. This paves the way for future research in geometric morphometrics and landmark recognition, as well as for the identification of incomplete wings.

3.2. Data preprocessing

Data issues in the dataset that pose an obstacle for successful models are displayed in various forms. These issues are the biological variability in tsetse flies, irregularities in image conditions, and human errors during annotation. This non-uniformity may be seen in the images as differences in orientation, focus, brightness, and overall image quality. These variations can influence how wing features are represented. The misalignment of images can create incomplete wings where the landmarks are obscured or missing entirely, causing inaccurate landmark detection and possible misclassification of wing types **[10]**.

To deal with these challenges, image pre-processing must be undertaken to standardise images and enhance their quality. Numerous image augmentation methods can synthetically increase the range of

the training dataset, enabling the model to learn broad representations from a limited data pool. Common augmentations include:

- Flipping right-wing images horizontally to resemble left wings, allowing the model to recognise anatomical characteristics for varied orientations without difficulty, effectively doubling the sample size.
- Rotating the images within a certain range allows the model to learn to expect changes in orientation, given that wings may be digitised at varying angles.
- Similarly, translating images vertically or horizontally adds further position variability to the pool, which trains the model to identify wings regardless of its cardinal positioning.
- Resizing images to fixed dimensions ensures uniform input sizes. Standardising images in this way introduces consistency in the data for reliable model training.
- Zooming into specific areas of an image highlights finer details, allowing the model to focus on key morphological features that may be instrumental in classification efficiency.
- Colour jittering introduces subtle variations in image brightness and contrast, which trains the model to be robust to changes in lighting.

Through these augmentative measures, the model is trained to deal with changes presented in real-world images, improving its ability to accurately classify incomplete wing samples.

3.3. Training

Since most incomplete wings are missing landmarks 4 or 6, the deciding factor between complete and incomplete was whether landmarks 4 and 6 were missing, like in the previous study **[10]**

The VGG16 model was pre-trained on the ImageNet dataset containing over one million images spanning 1,000 classes. Training on this extensive dataset teaches the model to generalise features from diverse datasets, improving its performance for the specific task of tsetse wing classification. Fine-tuning involved unfreezing the last layers of the pre-trained VGG16 model and re-training them on the for application on tsetse data.

Several layers in the VGG16 model were repurposed. The original fully connected layers were replaced with a fully connected layer consisting of a single output, followed by a sigmoid activation function to yield binary classification. Batch normalisation was used to stabilise and accelerate training, enhancing model performance. The model used a 3-channel input of size 224 x 224 pixels for compatibility with ImageNet pre-training configuration, enabling the VGG16 architectures feature extraction capacity.

The previously discussed 1,200-image sample training data with even class distribution was pre-processed by normalisation of image pixel values and resizing to fit the input layer. A data split of 60%, 20%, and 20% was chosen for training, validation, and testing, to ensure that the model was properly validated. Data augmentation, including random rotations, translations, zooming and colour jitter were implemented for a model robust against orientation and dataset scale shifts.

The Adam optimizer was used to establish a starting learning rate of 0.0001 with a Binary cross-entropy loss function. To optimize the model's parameters for best classification of the wing images, model fine-tuning over 30-epochs was applied with a batch size of 50 **[10]**. The PyTorch and torchvision libraries were accessed for model architecture and training.

For right wing classification of Volume 22, a best performing VGG16 model was implemented, with performance metrics decided by its precision of differentiating between complete and incomplete wings.

3.4. Results

Fine-tuning the VGG16 model with unfrozen weights produced a final model with the lowest validation score of 0.0034. The total runtime for model fine-tuning was 303.80 minutes, reflecting the models relatively quick application on large datasets.

Using the newly trained VGG16 model for classifying Volume 22 identified a total of 1,647 incomplete wings, 11.066% of the data. These incomplete wing's distribution was 1265 right wings (16.998%) and 382 left wings (5.133%).

The implementation of VGG16 model for wing classification took 68.97 minutes to complete, again displaying the models efficiently on sizable data.

3.5. Analysis

The resulting classification of the model displayed a reliable performance in distinguishing complete and incomplete wings, identifying 11.066% of wings as incomplete, where 16.998% of right wings and 5.133% of left wings were classified as incomplete. This imbalance has implications on damage distribution between left and right wings, which could influence the classifier's sensitivity and specificity in future applications. These outcomes align with previous research, which reported precision and accuracy at 95% **[10]**.

Training's execution timings were steady—about 120 seconds every epoch—which resulted in a total training length of about one hour. The general classification stayed consistent even if the imbalance in incomplete wings would have brought a bias in model training. Future studies should concentrate on correcting this imbalance by means of resampling methods or alternative data augmentation techniques, therefore enhancing the performance of the classifier still more.

4. Tier 2: Landmark detection model

4.1. ResNet50 Model

The ResNet50 model is a prominent CNN architecture specifically designed to address issues with deep networks, such as the vanishing gradient problem **[21]**. Consisting of 50 layers, the model uses residual learning through skip connections and residual blocks. This allows the gradients to spread across the network during backpropagation without devaluation, which is instrumental for learning complex mappings. The output of a residual block can be defined as:

$$H(x) = F(x) + x$$

where H(x) represents the residual block output, F(x) is the learned residual function, and x is the input. This formulation enhances the training and performance of deep networks.

For the detection of wing landmarks, the ResNet50 model was fine-tuned using weights pre-trained on the ImageNet dataset. This transfer learning approach uses previously learned hierarchical features, providing a robust foundation for feature extraction tailored to the distinctive characteristics of the wing morphology. The architecture is a combination of convolutional layers, batch normalisation, ReLU activation functions, and pooling layers, which work in conjunction to capture intricate spatial relationships.

4.2. Data preprocessing

The dataset errors previously discussed were addressed with the same preprocessing measures as these used in the classification tier. Each image was resized to a standard dimension of 224 x 224 pixels

to align with the ResNet50 input requirements and ensuring uniformity across the dataset. Right-wing images were normalised, horizontally flipped, applied with random rotations within a ±22-degree, translations, zooming and colour jittering.

4.3. Training

An existing ResNet50 model, developed and made available by the previous research **[10]**, was used in the landmark detection tier. The model architecture involved batch normalisation and activation functions such as ReLU. Its architecture was tailored for the regression task by removing the last two layers and replacing them with a randomly initialised convolutional layer and a fully connected layer with 22 outputs. These outputs represent the (x, y) coordinates of the 11 anatomical landmarks on tsetse wings. The original model was fine-tuned by unfreezing select layers to adapt the network for the nuances of the tsetse wing dataset.

The dataset used for training the model consisting of 2,420 distinct complete wing images sampled from Volumes 20 and 21, with landmarks accurately annotated and reviewed **[10]**. During training, a mean squared error (MSE) loss function was applied, defined mathematically as:

$$MSE = \frac{1}{n}\sum_{i=1}^{n}(y_i - \hat{y}_i)^2$$

where y_i represents the true values and $\hat{y}_i$ the predicted values. The Adam optimization function was used to train the model for 100 epochs for enhanced convergence **[10]**. Outliers were meticulously identified and filtered to refine model performance. Training encompassed a fixed split of the dataset, allocating 60% for training and 20% of each of the validation and test sets. The model uses a pre-trained ResNet50 network on ImageNet, for accelerated training due to previously learned features related to the tsetse wing images. Figure 4 provides a high-level illustration of the model.

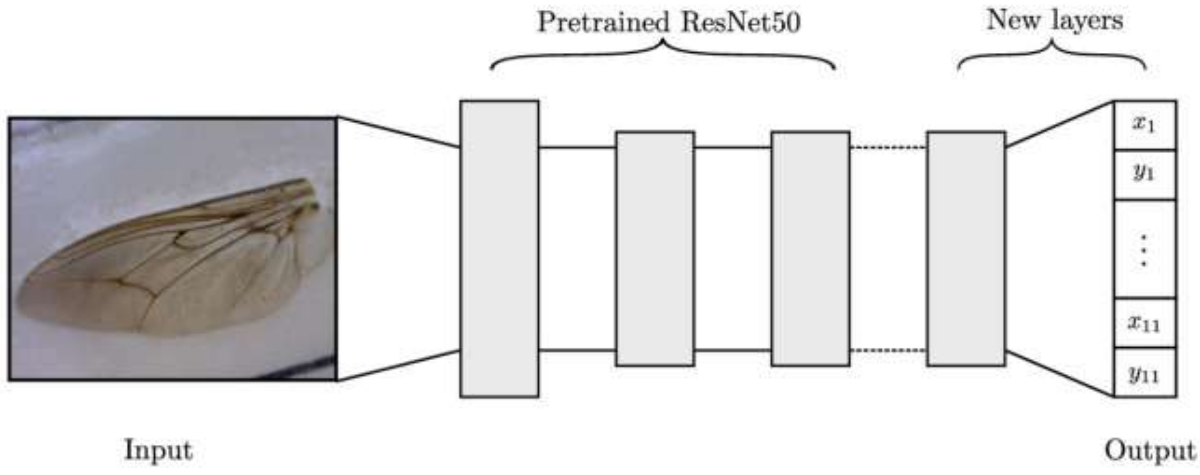

Figure 4: The ResNet50 model with modified final layers [10]

Key Python libraries involved in the process encompassed TensorFlow and Keras for model training, and NumPy and Pandas for data manipulation.

Morphometric data was produced by calculating distances between landmarks 1 and 6 for all complete right wings. A correlation analysis conducted on Volume 22 compared model predictions against manually measured wing lengths, using linear regression to calculate the R-squared and standard error scores. A scatter plot was structured to visualise the relationship between predicted and measured values.

Further correlation analyses were conducted across all individual pages of Volume 22 for a total of 377 individual plots, in which predicted right-wing lengths were compared to manually measured lengths. This collective approach has the potential to facilitate comprehensive validation of the model's predictive capabilities.

Landmarks were superimposed onto images from a sample of 4 pages using matplotlib and PIL libraries. This qualitative visualisation allowed for further validation of the predicted landmarks against actual wing images.

4.4. Results

The results from the ResNet50 model for landmark detection, which reached completion in a total runtime of 39.7 minutes, indicate strong performance across various analyses.

The model achieved an impressive linear regression correlation with R-squared score of 0.8459 when comparing predicted against manually measured wing lengths. This regression demonstrated a low standard error of 0.1781, indicating high reliability in the model's predictions. The scatter plot in Figure 5 depicts a strong clustering around the line of best fit, further validating the accuracy of the predictions.

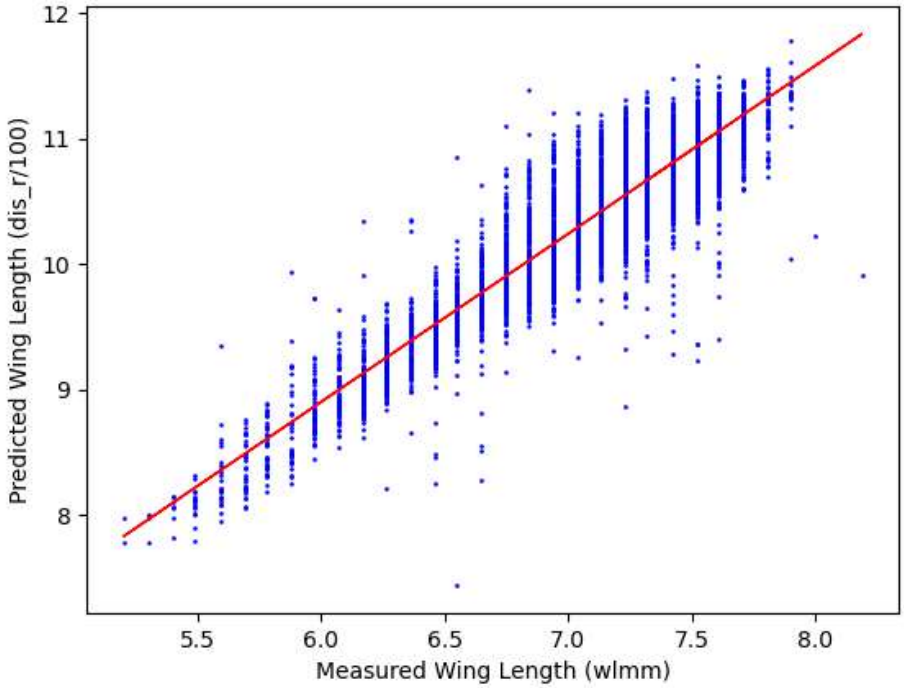

Figure 5: Correlation between the automatically detected wing length with the measured wing length of V22

The further correlation assessment on individual pages expanded upon these findings by conducting detailed correlation analyses across all 377 pages in Volume 22. Each individual plot revealed a generally high correlation between the predicted right-wing lengths from variable dis_r and the manual measurements from wlmm. For a subset of pages, scattered plots highlighted notable correlations with linear regressions. For instance, page 1155 shown in plot D of Figure 6b demonstrated exceptional alignment of predicted and measured lengths, which represented the majority of pages. Other page

plots indicated areas requiring further investigation due to lower correlations and the presence of outliers (Figure 6a-b). These findings underscore the robustness of the model's performance across different specimens.

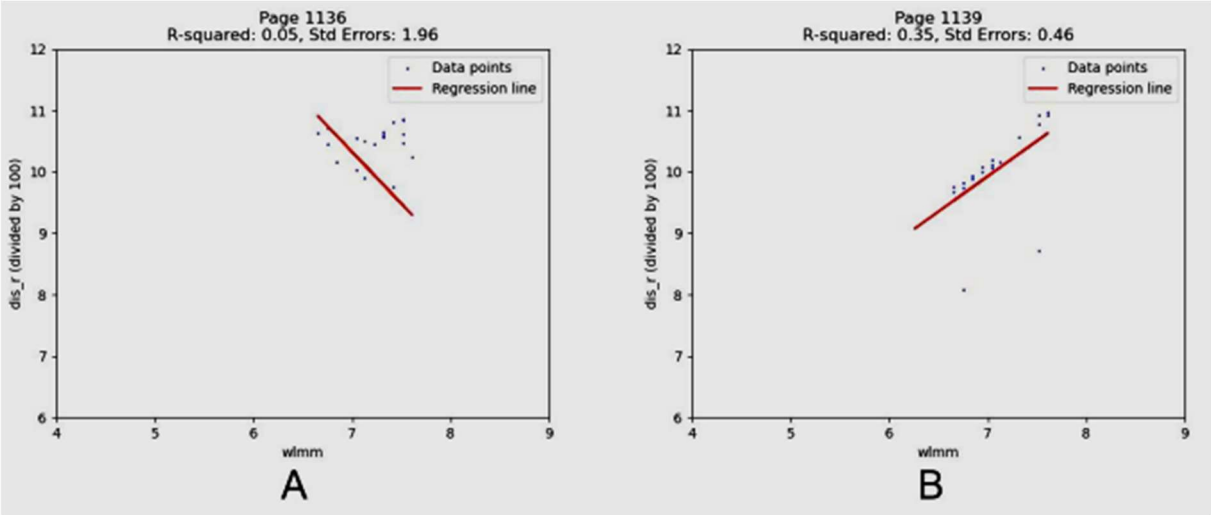

Figure 6a: Sample of linear regression plots of predicted (pixels) vs measured (mm) wing lengths for volume 22 pages.

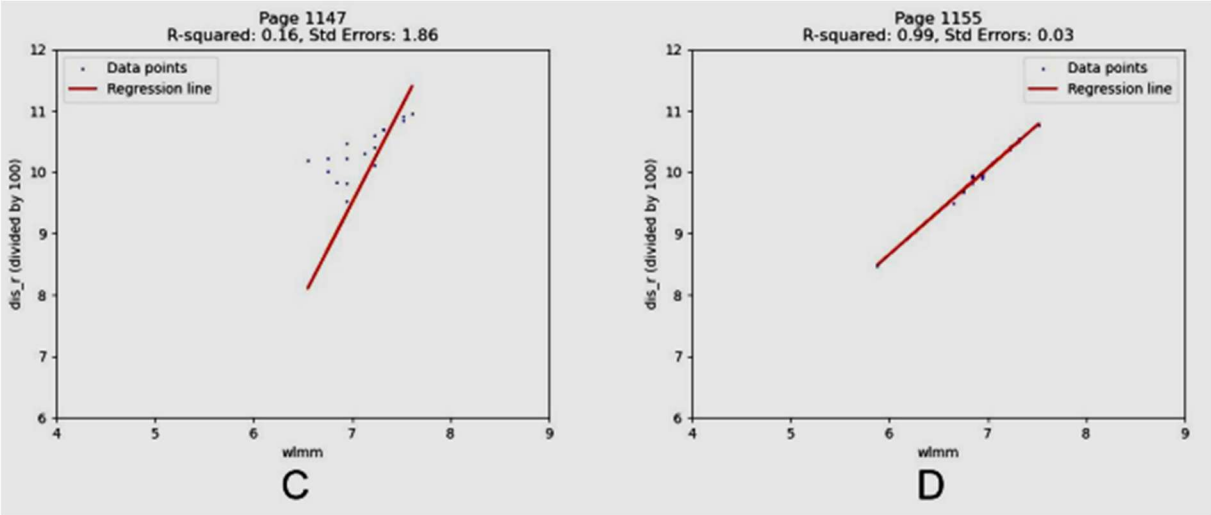

Figure 6b: Sample of linear regression plots of predicted (pixels) vs measured (mm) wing lengths for volume 22 pages.

Furthermore, the 11 predicted landmarks were superimposed onto the wing images of sample pages, resulting in 120 images showcasing a close alignment between the predicted landmark positions and their actual counterparts. Notably, the visual output provided compelling evidence of model effectiveness, particularly in complete wings, while occasionally highlighting discrepancies in cases of incomplete specimens. Figures 7 and 8 display a subset of the images with superimposed landmarks.

Figure 7a: Complete wing images with landmark predictions.

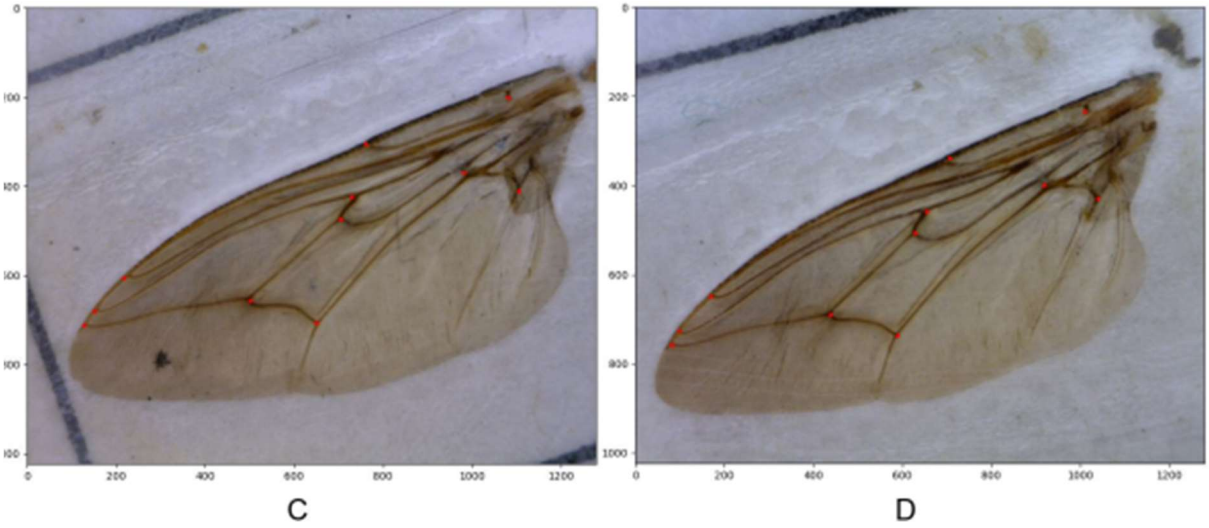

Figure 7b: Complete wing images with landmark predictions.

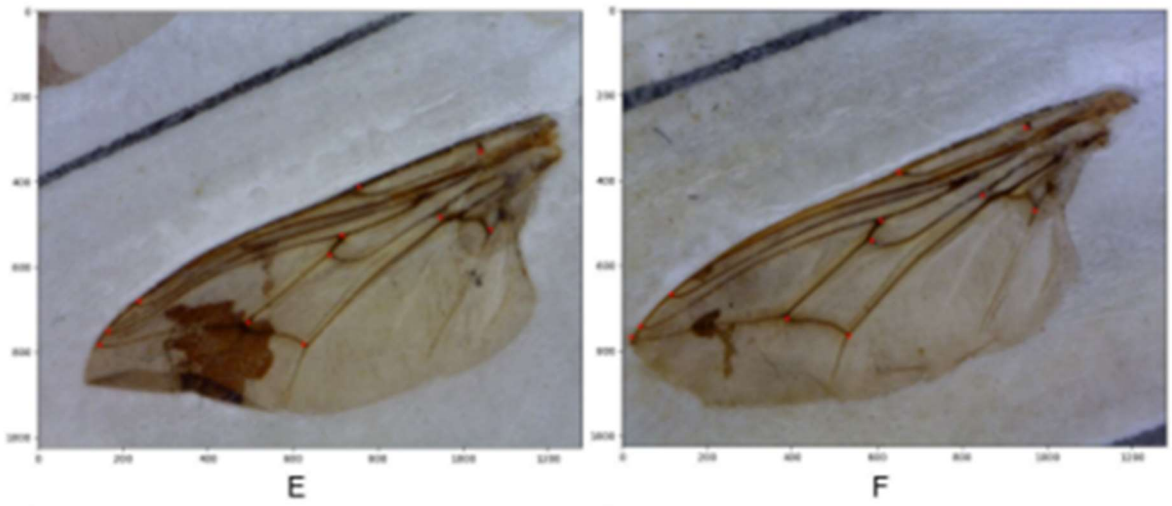

Figure 8a: Incomplete wing images with landmark predictions.

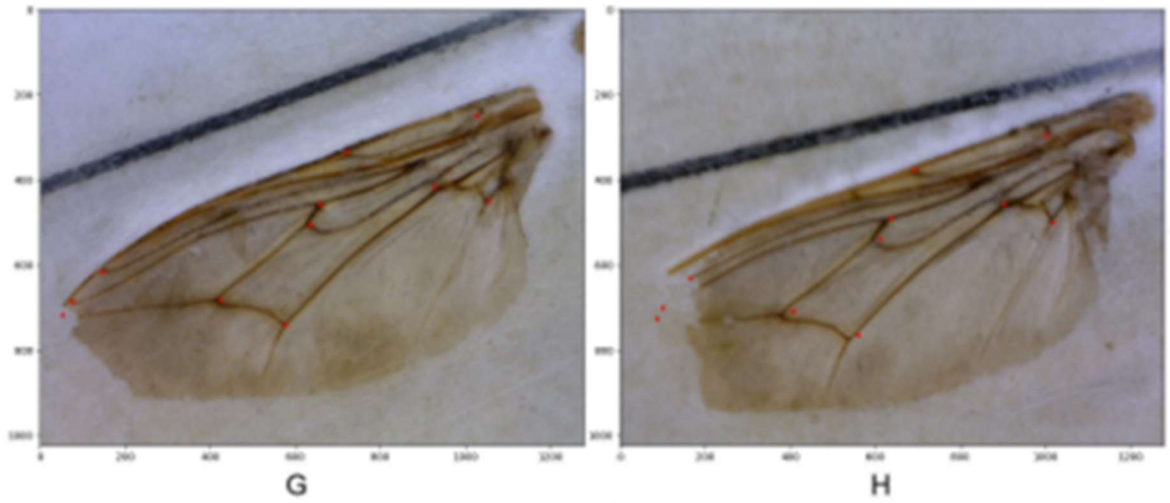

Figure 8b: Incomplete wing images with landmark predictions.

Figure 8c: Incomplete wing images with landmark predictions.

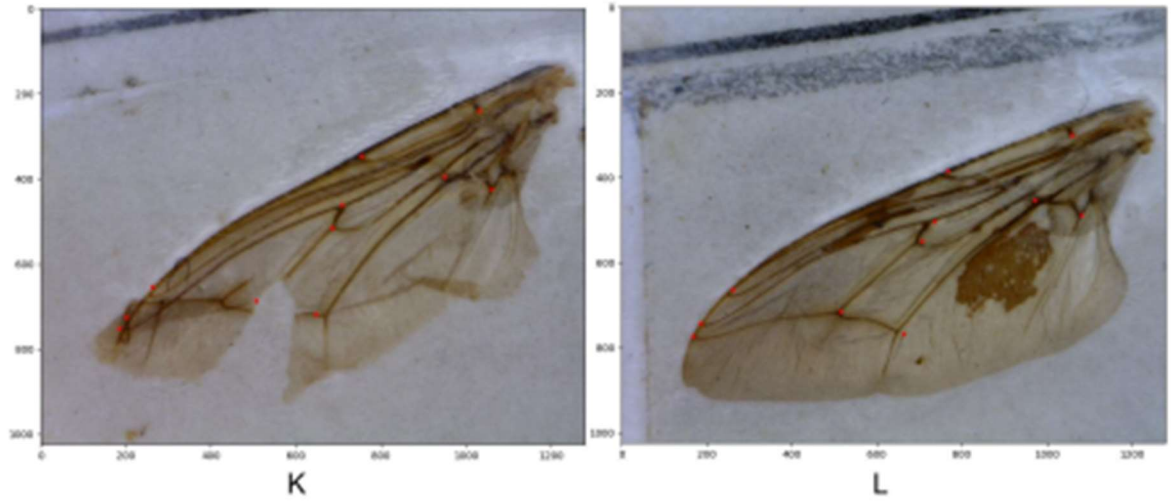

Figure 8d: Incomplete wing images with landmark predictions.

4.5. Analysis

The analysis of the landmark detection results emphasizes the strong performance of the ResNet50 architecture in predicting anatomical landmarks on tsetse fly wings. With an R^2 score of 0.8459, the model demonstrates a substantial ability to explain the variance in predicted wing lengths compared to manually measured data. This indicates that the model effectively captures the relationships inherent in the morphological features of the wings. The low standard error of 0.1781 further corroborates the model's reliability, suggesting that predictions are closely aligned with actual measurements.

Upon diving into the detailed per page correlation analyses, it was observed that the performance varied across the 377 pages analysed. While most of the scatter plots exhibited strong correlation, as representing in plot D, allowing clear visualisation of the predictive validity, subsets indicated challenges, like in plots A, B and C, particularly with low correlation and the presence of outliers on select pages. Identifying these discrepancies is crucial as they highlight areas for model refinement, potentially linked to imaging quality or occlusions affecting landmark visibility. These plots may show where there are errors in the results, either from the model predictions or the manual measurements. Further investigations could be conducted by inspecting individual pages that show poor correlation results. In this case, plot B's poor correlation may be explained by the 2 distinct outliers in the bottom right of the image.

Incorporating qualitative evaluations from the images superimposed with its landmarks, it was affirmed that predicted landmarks generally aligned well within sample wing images. The visual evidence of landmark superimpositions onto 120 images illustrates the model's capability, although cases of incomplete wings display more significant discrepancies. This suggests that the model's robustness may diminish when faced with challenging specimens that possess irregular features or structural damage.

Ultimately, the combined results across these analyses showcase the ResNet50 model's capability for accurate landmark detection. Continuous refinement of both the modelling techniques and the training datasets will be crucial for addressing these variabilities and enhancing the overall performance of the landmark detection system, ensuring its applicability for extensive morphometric studies across diverse biological datasets.

4.6. Deep learning comparison with related research

The landmark detection results in this study, using the ResNet50 model, demonstrate a significant improvement over previous methodology. Geldenhuys **[10]** achieved an R^2 score of 0.812 in their two-tier approach combining VGG16 for wing classification and ResNet50 for landmark regression, while the current study reports an R^2 score of 0.8459, affirming enhanced predictive power **[10]**. Additionally, the standard error of 0.1781 in the current model indicates greater reliability in landmark predictions.

In contrast, Leonardo **[20]** employed traditional image processing methods, achieving only approximately 75% accuracy in landmark detection. This further emphasizes the superiority of deep learning techniques, particularly the ResNet50 architecture, in accurately capturing intricate biological features and enhancing performance in landmark detection tasks. The advancements made in this study illustrate a substantial leap in the efficacy of automated landmark detection compared to both prior studies **[10, 20].**

5. Morphometric analyses

5.1. Data Description

Data used for morphometric analyses was the accumulated data from volumes 20, 21 and 22. The biological and morphometric data from volumes 20 and 21 came from Geldenhuys' study. The data subset Geldenhuys worked with consisted of 14,354 pairs of tsetse wings collected over nearly two years, capturing seasonal variations and environmental conditions **[10]**. For consistency in further analyses, all measured wing lengths wlm were converted to millimetres.

Cumulatively, V20-22 were collected from Nov 1994 until Feb 1997, consisting of 22051 flies/lines and a maximum of 44102 wings. There were 2 accompanying spreadsheets, the first containing the biological and morphometric data for V20-22 had 22051 row instances per fly, and variables pertaining to the morphometric analyses are listed in Table 2.

Table 2: Biological data captured in lab dissection

Variable	Description
vpn	Volume, page and number, e.g. 22077904
cd	Day of the month that fly was recorded
cm	Month of the year that fly was recorded
cy	Year that fly was recorded
g	Genus of the fly: 'Gp' for *G. pallidipes* or 'Gmm' for *G. m. morsitans*
s	Sex: 1 for male, 2 for female
hc	1 if hatchet cell used, 0 if distance landmarks 1 to 6 used
wlm	manually measured ring wing length from landmarks 1 to 6 in mm, otherwise hatchet length
f	Wing fray category, also approximates age [1 – 6]
lmkr	Number of landmarks missing on right wing: 1 – 11
right_good	0 for complete right wings, 1 for incomplete right wings
dis_r	automatically predicted right wing length from landmarks 1 to 6 in mm, otherwise hatchet length

The second spreadsheet contained the environmental data recorded every day during the time of the tsetse collection at the Rekomitjie Research Station, spanning 2,967 days, from 17 Nov 1991 until 31 Dec 1999. The variables are listed in Table 3.

Table 3: Biological data captured in lab dissection

Variable	Description
Date	Day of environmental info collection
tbar	Average temperature
tmax	Maximum temperature
avrh	Average relative humidity
minrh	Minimum relative humidity
avsdmB	Average solar radiation
maxsdmB	Maximum solar radiation
ndvi	Normalized Difference Vegetation Index
rain	Depth of water from rain in mm

5.2. Data pre-processing

The combined dataset had a total of 22,051 right wing specimens, where 19,387 of them were classified as complete and 2,664 as incomplete for 12.081%. In preparation for a time-series analysis, only the flies which corresponded to complete right wings were considered. Further exclusions included 76 specimens in the data that:

- had a predicted wing lengths missing due to error,
- were measured by their hatchet cell, usually due to damaged landmarks,
- had more than 2 missing landmarks.

For the remaining 19,311 complete specimens, the linear regression between measured and predicted wing lengths was determined. Subsequently, outlier detection was conducted, where outliers are more than 3 standard deviations from the mean. A total of 588 outliers were detected, or 3.044% of complete right wings were outliers. After these exclusions, 18,723 wing specimens without errors remained. The extreme outliers lying outside 5 standard deviations were also identified, with a total of 118 extreme outlier specimens.

In Figure 9, the linear regression between measured and predicted wing lengths are plotted, where the 18,723 inliers are coloured blue, and the 588 outliers are coloured orange and red, where red are the 118 extreme outliers.

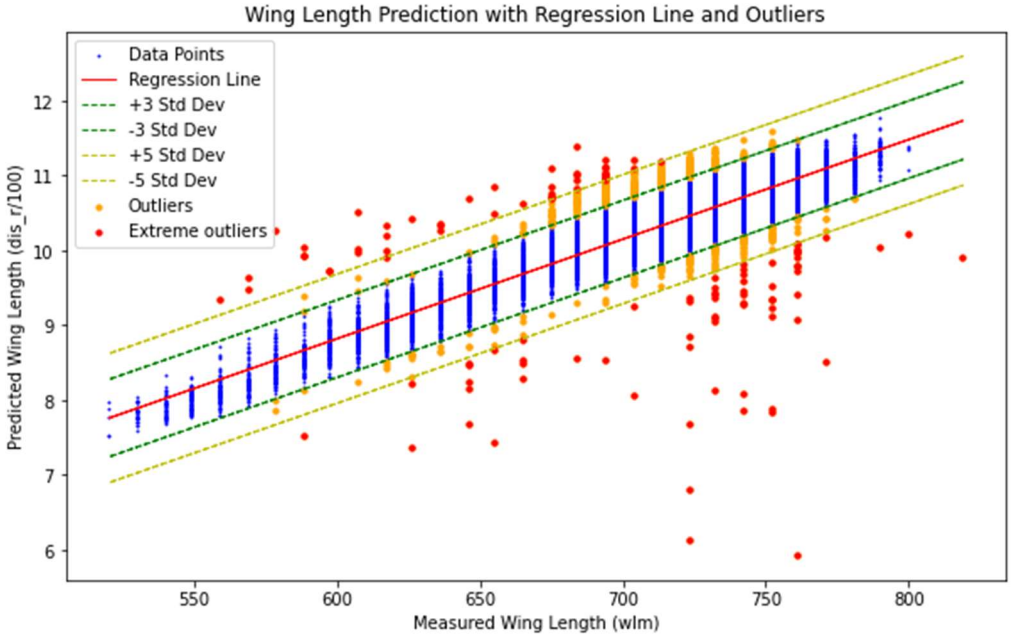

Figure 9: The linear regression between predicted and measured wing length of V20-22 with outlier exclusion

5.3. Time-series analysis

5.3.1. Wing lengths vs time

Time series experiments were conducted using the reduced wing length data and corresponding environmental variables. Daily averages and standard deviations of wing lengths were calculated and merged with environmental data, resulting in 515 data points representing each fly collection day.

The analysis employed Lowess Smoothing, a non-parametric method fitting multiple regressions in local neighbourhoods, to visualize wing length trends over the 515-day collection period. This approach revealed subtle fluctuations and potential seasonal patterns in wing morphology.

Figure 10 shows the change in wing length through time with one standard deviation.

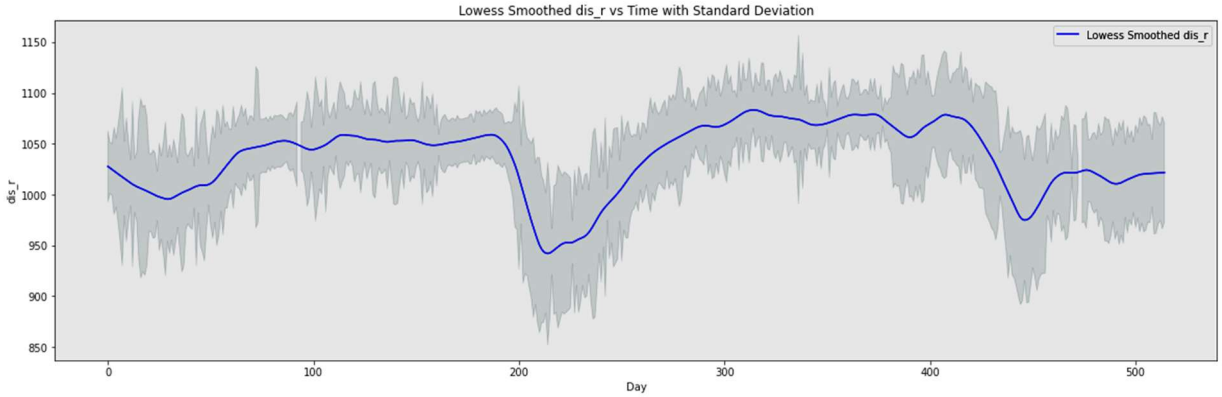

Figure 10: The average tsetse wing length recorded in Zimbabwe over 515 days.

The time series analysis revealed both short-term fluctuations and longer-term trends in wing length, suggesting complex interactions between tsetse fly morphology and environmental variables over time. These findings lay the groundwork for more detailed investigations into the ecological and evolutionary implications of wing morphology changes in tsetse fly populations.

5.3.2. Influence of environmental variables on wing length

The influence of environmental variables on wing length was examined through a comprehensive time-series analysis. For the analysis, the daily average wing lengths spanning the fly collection period was compared with corresponding environmental data, resulting in 515 observations. The Lowess Smoothing method was applied to visualize the change in wing length over time, revealing distinct patterns of variation.

A correlation analysis of the environmental variables versus average wing lengths was conducted, which gave these results:

- tbar: Pearson correlation = -0.607, p-value = 0.000
- tmax: Pearson correlation = -0.542, p-value = 0.000
- avrh: Pearson correlation = 0.205, p-value = 0.000
- minrh: Pearson correlation = 0.182, p-value = 0.000
- avsdmB: Pearson correlation = -0.450, p-value = 0.000
- maxsdmB: Pearson correlation = -0.446, p-value = 0.000
- ndvi: Pearson correlation = 0.222, p-value = 0.000
- rain: Pearson correlation = -0.060, p-value = 0.173

According to strength of correlation with wing length, the variables in order of most to least impactful were: tbar, tmax, avsdmB, maxsdmB, ndvi, avrh, minrh, and rain.

The correlations uncovered significant relationships between environmental variables and average wing lengths. Temperature showed a negative correlation with wing length, suggesting warmer

conditions may influence wing development. Conversely, humidity exhibited a positive correlation, indicating potential adaptive responses to moisture levels.

Each variable is plotted next to wing length through time in Figures 11a-h below:

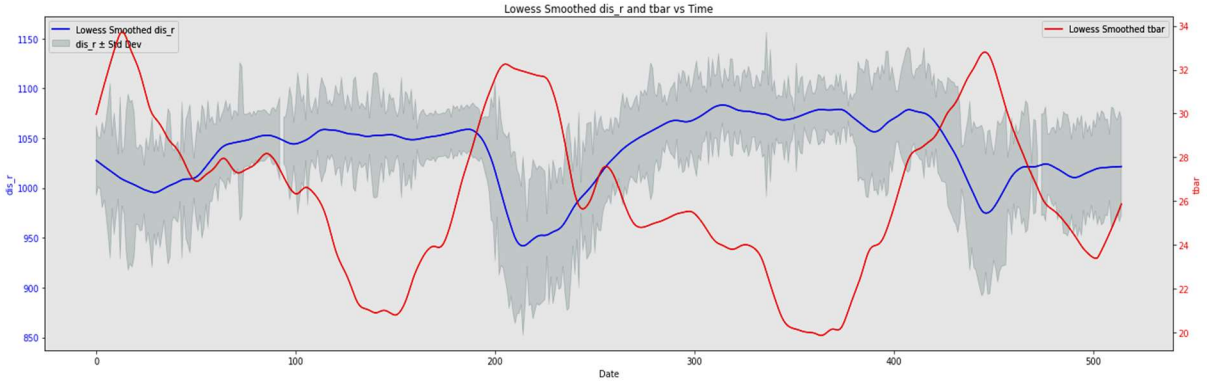

Figure 11a: Wing length vs Average temperature

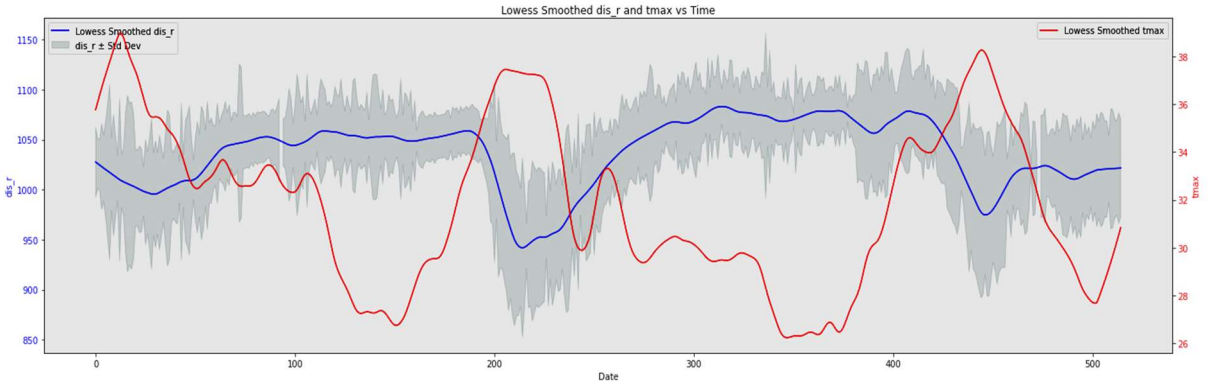

Figure 11b: Wing length vs Maximum temperature

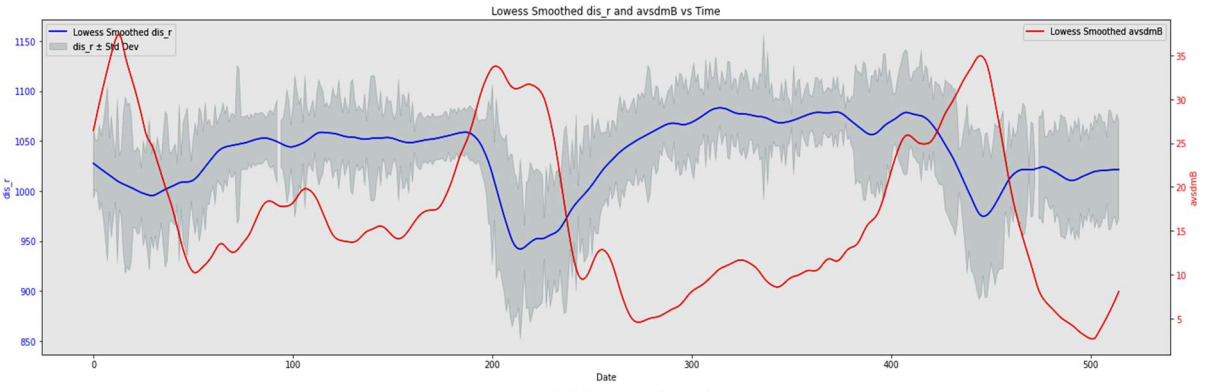

Figure 11c: Wing length vs Average solar radiation

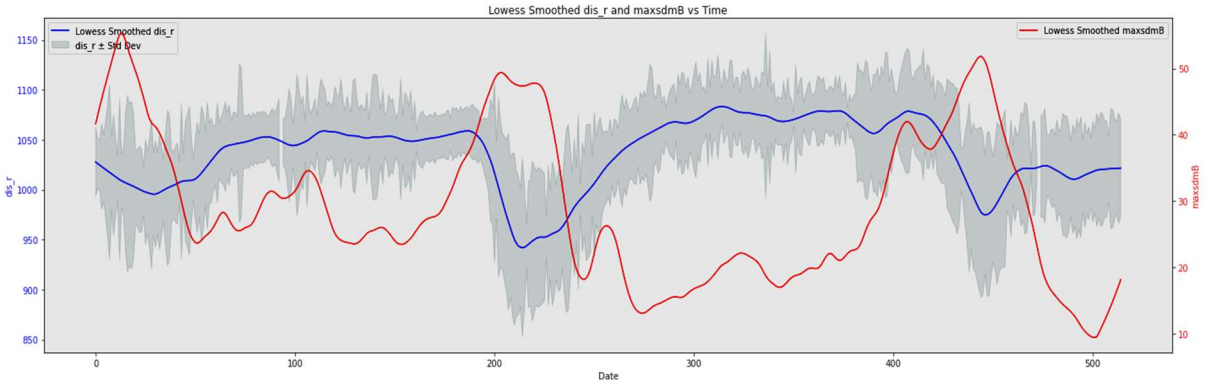

Figure 11d: Wing length vs Maximum solar radiation

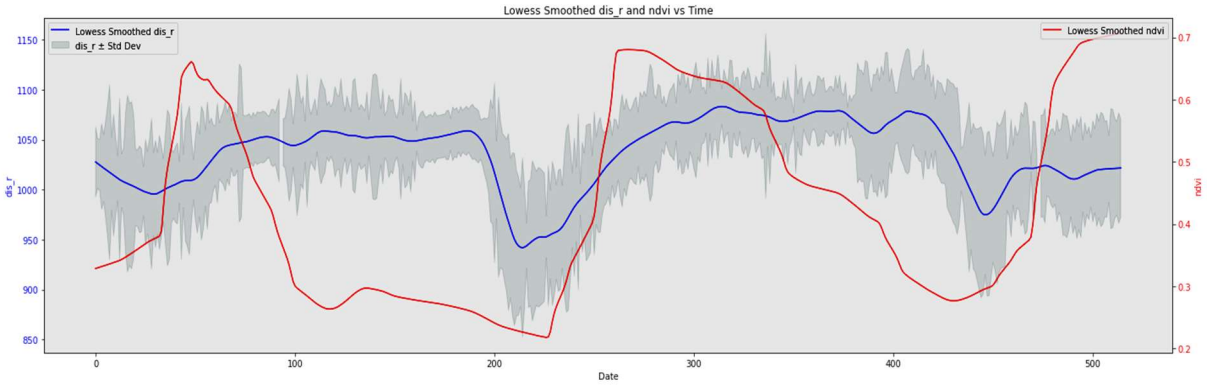

Figure 11e: Wing length vs Normalized Difference Vegetation Index

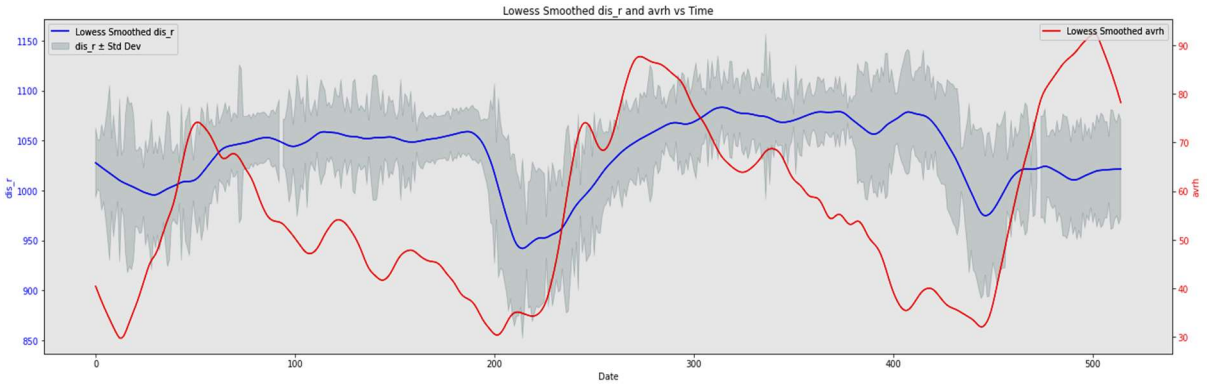

Figure 11f: Wing length vs Average relative humidity

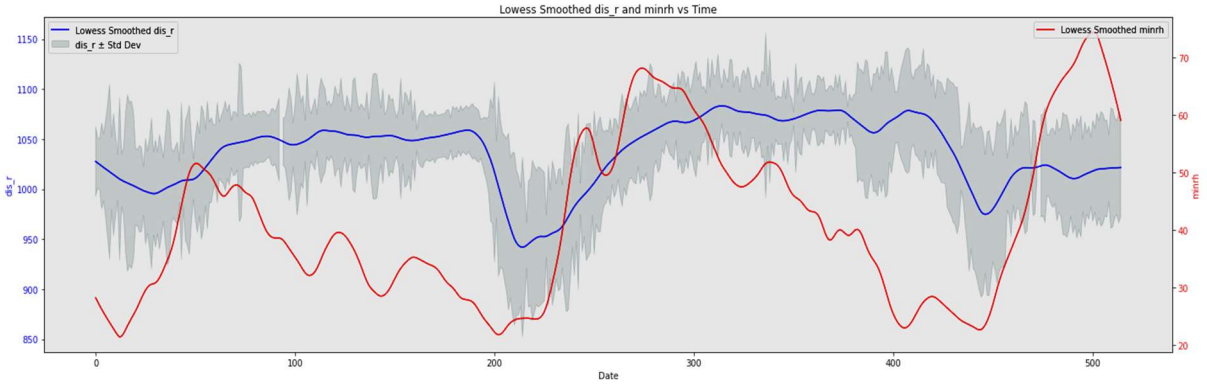

Figure 11g: Wing length vs Minimum relative humidity

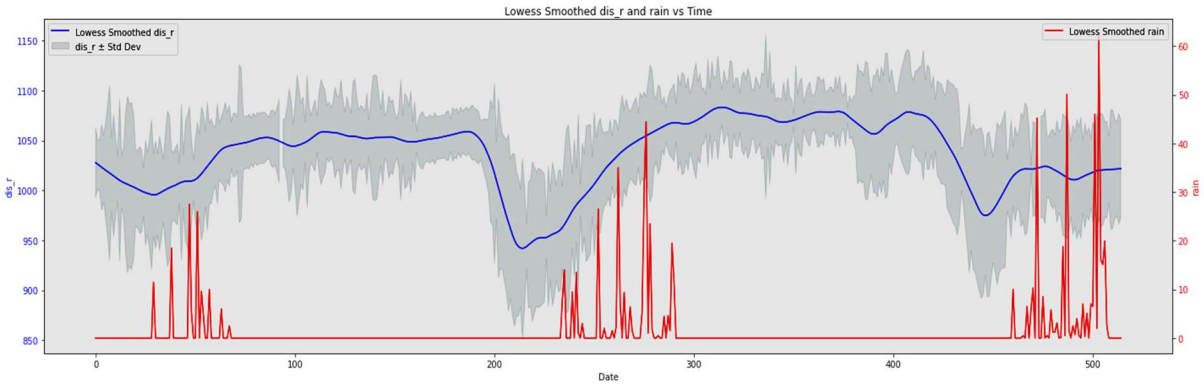

1. **Figure 11h:** Wing length vs Rainfall in mm

6. Time-series comparison with related research

A comprehensive correlation analysis was conducted to assess the relationship between environmental variables and wing length. The analysis revealed several significant correlations:

1. Temperature: A negative correlation was observed between temperature and wing length, suggesting that warmer conditions may adversely affect wing development, possibly due to physiological stress on developing pupae.

2. Humidity: Conversely, humidity levels showed a positive correlation with wing length. Higher moisture levels appeared to promote increased wing size. This relationship was particularly pronounced during certain seasons.

3. Rainfall: Short-term increases in rainfall were associated with temporary decreases in wing length. However, over longer periods, increased rainfall correlated with larger wing sizes. These patterns should be investigated to properly understand the cause.

4. Vegetation index: A positive correlation was found between vegetation indices and wing length, suggesting that improved habitat quality leads to larger wing sizes.

These findings align with the other studies **[9, 10]**, whose work emphasised the role of environmental factors in shaping tsetse fly morphology. The complex interplay between these variables highlights the adaptive capacity of tsetse flies to varying environmental conditions.

Seasonal trends were evident, with distinct patterns of wing length variation corresponding to wet and dry seasons. The magnitude of these seasonal effects often outweighed other factors **[9]**, where seasonal variations were found to be up to 20 times greater than effects from capture methods.

The analysis also revealed potential lag effects, where environmental conditions during pupal development influenced adult wing morphology **[9]**. This suggests that the impact of environmental variables extends beyond immediate effects and may have long-term consequences for population dynamics.

These findings have important implications for understanding tsetse fly ecology and evolution. The observed morphological plasticity in response to environmental variables indicates that tsetse populations may have the capacity to adapt to changing climatic conditions. However, the complex

nature of these relationships also suggests that predicting the long-term impacts of climate change on tsetse populations will require careful consideration of multiple interacting factors.

7. Discussion and Conclusion

The primary objective of this study was to examine the morphological characteristics of tsetse flies, with a particular emphasis on the fluctuations in wing length in response to environmental factors. To achieve this, we compiled a comprehensive dataset that encompassed biological, morphometric, and environmental data that was collected over a period of several years. From this dataset, we initiated our morphometric studies, which also enabled a comprehensive examination of the relationships between the morphology of tsetse flies and their ecological environment.

The data from volumes 20, 21, and 22, which were collected from November 1994 to February 1997, were utilized in our analysis, which included 22,051 flies and up to 44,102 wings. This extensive dataset captured seasonal fluctuations and environmental conditions, thereby providing a robust foundation for our research. All recorded wing lengths were translated from millimetres to ensure uniformity in future investigations.

Our research primarily concentrated on the implementation of a two-tier Convolutional Neural Network (CNN) model, as per Geldenhuys' (2023) research. The objective of this innovative method was to enhance the precision of morphometric measures by automating wing image analysis. The initial level of the CNN focused on the classification of wings as either complete or partial, thereby excluding specimens that were damaged. The second stratum projected landmark coordinates using the identified entire wings, thereby simplifying the analysis procedure, and ensuring consistency in the count of landmarks across all samples.

The performance of the two-tier CNN method was quite exceptional. We successfully generated landmarks on a vast collection of tsetse wing images by placing 11 anticipated landmarks on 120 sample wing photos. This visual output provided compelling evidence of the model's efficacy, particularly in the case of entire wings. The method demonstrated exceptional accuracy in estimating wing lengths and landmark positions by significantly reducing the time and effort required for manual measurements.

Our findings have substantial implications for the field of morphometric analysis in ecological research. The successful application of deep learning methods to analyse tsetse fly wings establishes a new standard for data processing in this field. By automating the landmark detection process, we have enhanced the efficacy of data collection and the dependability and consistency of morphometric measures.

The integration of conventional morphometric techniques with machine learning has significantly enhanced our ability to investigate tsetse fly populations. This method enables the processing of larger datasets with greater precision, thereby expanding the possibilities for understanding the adaptive responses of tsetse flies to environmental changes. Additionally, the methodology we developed could be adapted to facilitate comparable investigations on various insect carriers, thereby fostering broader advancements in the field of vector-borne disease research.

Our investigation of the morphology of tsetse fly wings yielded a significant new comprehension of the relationship between environmental conditions and wing form. Using a vast collection of over 22,000 specimens, we demonstrated the adaptive adaptability of tsetse fly populations by observing distinct patterns of variation in wing length across seasons and the years.

This investigation yielded numerous significant findings. Wing lengths exhibited cyclical patterns, with significant increases during the rainy season and declines during the drier season. This is in accordance with other research that suggests that environmental factors significantly influence the morphology of insects. Significant correlations were observed between wing length and other environmental variables:

Temperature: A positive correlation suggests that increased temperatures may encourage the development of larger wings, thereby enhancing dispersal capacity and flight performance.

A negative correlation implies that excessive moisture may impede wing growth, potentially because of physiological duress during the pupal stage.

Vegetation Index: A favourable correlation between habitat quality and larger wing sizes is the result.

The dynamic character of tsetse fly populations and their responses to changing environmental conditions are underscored by year-to-year variations in wing lengths, particularly in cases of non-overlapping confidence intervals. The discovery that environmental factors during pupal development influence adult wing morphology suggests that the influence of environmental variables may have long-term ramifications for population dynamics, in addition to instantaneous impacts.

These findings have numerous substantial implications:

The observed morphological flexibility in response to environmental factors implies that tsetse populations may have the capacity to adapt to the changing seasons. This adaptation may impact their survival and distribution patterns in response to environmental change.

Understanding the relationship between environmental factors and wing form is essential for the development of more effective vector control techniques. Targeting control activities during seasons or conditions that are conducive to larger wing diameters, for instance, may be more effective in reducing tsetse fly populations.

The potential responses of tsetse fly populations to future climate conditions are inferred from the strong correlations between wing form and environmental factors. This knowledge is essential for predicting potential changes in the distribution and abundance of tsetse flies in the context of numerous climate change forecasts.

Ecological Modelling: The capacity to predict the distribution and behaviour of tsetse fly populations in various habitats can be significantly enhanced using comprehensive morphological data and its relationships with environmental parameters.

Evolutionary Insights: The observed morphological variances and their environmental implications significantly improve our understanding of insect adaptation and speciation, providing a detailed analysis of the evolutionary processes that shape tsetse fly populations.

In conclusion, the two-tier CNN approach has facilitated a more thorough and efficient examination of the morphology of tsetse flies, thereby emphasizing the potential of machine learning methods to revolutionize data analysis in ecological research. This two-tier approach substantially enhances our understanding of the biology of tsetse flies and its implications for vector control policies. Furthermore, the morphological investigation has established a robust foundation for understanding the adaptive significance of variations in wing length in tsetse flies. We have not only enhanced our comprehension of tsetse fly ecology by elucidating the complex relationship between environmental factors and morphological characteristics, but we have also contributed insightful analysis to the broader fields of vector biology and insect evolution.

Even though this study provides significant new insights into the forms of tsetse fly wings and their interactions with environmental factors, it is necessary to acknowledge certain limitations.

Initially, the dataset, despite its size, is limited to specific geographical regions and time periods, which would not accurately represent the diversity of tsetse populations across multiple habitats or climatic conditions. The results' relevance to contemporary situations may be influenced by the fact that the data collection period, which spanned from November 1994 to February 1997, may not accurately reflect current environmental conditions or tsetse fly populations.

Secondly, the study primarily focused on wing length as the primary morphological characteristic, potentially omitting other critical aspects of tsetse fly morphology that are influenced by environmental conditions. This restricted emphasis may limit our understanding of the complete range of morphological adaptations in tsetse flies.

Thirdly, the automatic landmark detection technology introduced potential sources of inaccuracy, despite its increased efficiency. The system may have misclassified certain wings or incorrectly positioned landmarks, particularly those with unusual shapes or damage. This may result in bias in the morphometric investigation, particularly for wing forms at the extremities of the distribution.

Lastly, the study's dependence on a limited number of ambient factors may result in an oversimplification of the complex relationships that influence the shape of wings. Other factors, such as genetic variability, predation pressures, and interspecific competition, were not accounted for, potentially leading to an insufficient understanding of the underlying causes of morphological changes in tsetse fly populations.

This study's innovative approach to automated landmark detection in tsetse fly wings suggests intriguing avenues for future research. One promising approach is to broaden the scope of the investigation to include a broader range of tsetse species and populations across multiple geographical regions. This would offer a more comprehensive understanding of the correlation between environmental elements and morphological variances.

In the future, research could also focus on the heritability of wing shape features and their potential role in local adaptation through the integration of our morphometric data with genetic analyses. This can assist in the elucidation of the evolutionary mechanisms that influence the populations of tsetse flies in response to varying environments.

Prediction model development Another critical area of future research is the integration of our morphometric findings with climatic data to predict potential changes in the distribution and behaviour of tsetse flies in response to various climate change scenarios. This could be quite beneficial in predicting and mitigating future risks associated with the transmission of diseases.

The automated landmark detecting method developed in this study has potential applications beyond the tsetse fly. Adapting this approach to various insect carriers will enable us to gain a more comprehensive understanding of the dynamics of vector-borne diseases across a variety of species.

Our findings have substantial implications for the management of tsetse flies in the real world. By providing insights into the interaction between environmental conditions and wing morphology, this study can serve as a guide for more focused and successful vector control initiatives. The development of sustainable solutions to combat trypanosomiasis is contingent upon an understanding of the way tsetse fly populations adjust to changing environments, thereby promoting improved human and animal health in affected regions.

8. Acknowledgements

In this study, the ChatGPT AI was used for revision of research content, to ensure a formal tone is used. All of the research results and processes are the authors own original work.

9. References

[1] Dujardin JP, Slice DE. (2007) Contributions of morphometrics to medical entomology. *Encyclopedia of Infectious Diseases: Modern Methodologies*, M. Tibayrenc (Ed.) 17:435-47. https://doi.org/10.1002/9780470114209.ch25

[2] WHO Trypanosomiasis, human African (sleeping sickness). 2023. Available from: https://www.who.int/news-room/fact-sheets/detail/trypanosomiasis-human-african-(sleeping-sickness)/

[3] FAO Programme Against African Trypanosomosis (PAAT). 2024. Available from: https://www.fao.org/paat/the-programme/the-disease/en/

[4] Kaba D, Berté D, Ta BTD, Tellería J, Solano P, Dujardin JP. (2017) The wing venation patterns to identify single tsetse flies. *Infection, Genetics and Evolution* 47:132-9. https://doi.org/10.1016/j.meegid.2016.10.008 PMID: 27765637

[5] Vale GA, Hargrove JW, Solano P, Courtin F, Rayaisse J-B, Lehane MJ. (2014) Explaining the host-finding behavior of blood-sucking insects: computerized simulation of the effects of habitat geometry on tsetse fly movement. *PLoS Negl Trop Dis* 8(6): e2901. doi:10.1371/journal.pntd.0002901

[6] Ta BTD, Rayaisse JB, Salou E, Solano P, Dujardin JP. (2021) Tsetse flies: comparative morphometric information from traits collected on wings and pupae. *African Entomology* 29(2):522-33. https://doi.org/10.4001/003.029.0522

[7] Bursell E, Billing KC, Hargrove JW, McCabe CT, Slack E. (1974) Metabolism of the bloodmeal in tsetse flies (a review). *Acta Tropica* 31(4):297-310. PMID: 4155596

[8] Hargrove JW, Packer M. (1993) Nutritional states of male tsetse flies (Glossina spp.) (Diptera: Glossinidae) caught in odour-baited traps and artificial refuges: models for feeding and digestion. *Bulletin of Entomological Research* 83(1):29-46. https://doi.org/10.1017/S0007485300041754

[9] Hargrove JW, English S, Torr SJ, Lord J, Haines LR, Van Schalkwyk C, et al. (2019) Wing length and host location in tsetse (Glossina spp.): implications for control using stationary baits. *Parasites & Vectors* 12(1):1-3. https://doi.org/10.1186/s13071-018-3274-x PMID: 30635017

[10] Geldenhuys DS, Josias S, Brink W, Makhubele M, Hui C, Landi P, et al. (2023) Deep learning approaches to landmark detection in tsetse wing images. *PLoS Comput Biol* 19(6):e1011194. https://doi.org/10.1371/journal.pcbi.1011194

[11] Jackson CHN. (1946) An artificially isolated generation of tsetse flies (Diptera). *Bull Entomol Res* 37:291–9. https://doi.org/10.1017/s0007485300022203

[12] Dujardin JP. (2008) Morphometrics applied to medical entomology. *Infection, Genetics and Evolution* 8(6):875-90. https://doi.org/10.1016/j.meegid.2008.07.011

[13] Dujardin JP, Dujardin SD. (2019) Geometric morphometrics in the cloud. *Infection, Genetics and Evolution* 70:189-96. https://doi.org/10.1016/j.meegid.2019.02.018

[14] Jordan MI, Mitchell TM. (2015) Machine learning: Trends, perspectives, and prospects. *Science* 349(6245):255-60. https://doi.org/10.1126/science.aaa8415 PMID: 26185243

[15] Simonyan K, Zisserman A. (2015) Very Deep Convolutional Networks for Large-Scale Image Recognition. *Computer Vision and Pattern Recognition* (arXiv). https://doi.org/10.48550/arXiv.1409.1556

[16] Geldenhuys D. (2023) Tsetse fly wing landmark data for morphometrics (Vol 20, 21), *Dryad*, Dataset. https://doi.org/10.5061/dryad.qz612jmh1

[17] Geldenhuys D, Josias S. (2023) Landmark detection for tsetse fly wings (Version 1.0.4) [Computer software]. Available from https://github.com/DylanGeldenhuys/Landmark-detection-for-tsetse-fly-wings

[18] Ryklief MN. (2024) Tsetse Wing Morphology Dynamics: Automated Landmark Detection and Time Series Analysis (Vol 22), *Dryad*, Dataset. https://doi.org/10.5061/dryad.wstqjq2wv

[19] Ryklief MN. (2024) Tsetse Wing Morphology Dynamics: Automated Landmark Detection and Time Series Analysis [Computer software]. Available from https://github.com/NuhrRyklief/Tsetse-Wing-Morphology-Dynamics

[20] Leonardo MM, Carvalho TJ, Rezende ER, Zucchi RA, Faria F. (2018) Deep Feature-Based Classifiers for Fruit Fly Identification (Diptera: Tephritidae). *2018 31st SIBGRAPI Conference on Graphics, Patterns and Images* (SIBGRAPI):41-47. https://doi.org/10.1109/SIBGRAPI.2018.00012

[21] He K, Zhang X, Ren S, Sun J. (2015) Deep residual learning for image recognition. *Computer Vision and Pattern Recognition* (arXiv). https://doi.org/10.48550/arXiv.1512.03385

[22] Torr SJ, Hargrove JW. (1999) Behaviour of tsetse (Diptera: Glossinidae) during the hot season in Zimbabwe: the interaction of micro-climate and reproductive status. *Bulletin of Entomological Research* 89(4):365-79. https://doi.org/10.1017/S0007485399000504

[23] Animal Wildlife: 10 Interesting Tsetse Fly Facts and Pictures [Image]. 2012. Available from: https://animal-wildlife.blogspot.com/2012/01/10-interesting-tsetse-fly-facts.html